ELSEVIER

Journal of Photochemistry and Photobiology A: Chemistry 145 (2001) 145–157

Journal of Photochemistry and Photobiology A:Chemistry

www.elsevier.com/locate/jphotochem

Structure property relations of photoreactive polymers designed for laser ablation

T. Lippert [a,*], C. David [a], J.T. Dickinson [b], M. Hauer [a], U. Kogelschatz [c], S.C. Langford [b], O. Nuyken [d], C. Phipps [e], J. Robert [b], A. Wokaun [a]

[a] *Paul Scherrer Institut, 5232 Villigen PSI, Switzerland*
[b] *Washington State University, Pullman, WA 99164-2814, USA*
[c] *ABB Corporate Research Ltd., 5405 Baden, Switzerland*
[d] *Technische Universität München, Lichtenbergstr. 4, 85747 Garching, Germany*
[e] *Photonic Associates, 200A Ojo de la Vaca Road, Santa Fe 87504, USA*

Abstract

The ablation characteristics of various polymers were studied at low fluences, and structure property relations were obtained. The polymers containing the photochemically most active group (triazene) are also the polymers with the lowest threshold of ablation and the highest etch rates, followed by a designed polyester and then polyimide. No pronounced influences of the absorption coefficients, neither α_{lin} nor α_{eff}, on the ablation characteristics are detected. The thermal properties of the designed polymers are only of minor importance. Intensities of fragments obtained by time-of-flight mass spectrometry measurements show pronounced differences between irradiation at the absorption band of the triazene group (308 nm) and irradiation at a shorter wavelength (248 nm). The larger fragments reveal lower intensities for 248 nm irradiation, due to the additional decomposition of these fragments by the higher energy of 248 nm photons and the lower etch rates for 248 nm irradiation. An excimer lamp emitting at 308 nm is applied to decompose the triazene group without major decomposition of the aromatic system. Irradiation with shorter wavelengths, i.e. 222 and 172 nm, causes in addition the decomposition of the aromatic system. Two novel applications for the special designed photopolymers are shown. These polymers can be applied in combination with phase masks for the fabrication of microoptical elements using laser ablation. Another quite different application utilizes near-IR irradiation. The plasma created by laser ablation acts as a micro thruster. © 2001 Elsevier Science B.V. All rights reserved.

Keywords: Photopolymer; Ablation; TOF-MS; Excimer lamps; Microoptic; Phase mask; Laser plasma thruster

1. Introduction

Laser ablation of polymers was first reported in 1982 [1,2] and envisioned as a possible alternative or complementary technique to conventional photolithography, but has unfortunately several disadvantages, i.e. low sensitivity [3], carbonization upon irradiation [4], and debris contaminating the surface and optics. Many of these disadvantages of laser ablation, compared to conventional photolithography, are the result of the application of standard polymers. These polymers are designed for totally different applications, but have to compete with the highly specialized photoresists and photolithographic processes. Therefore, novel photopolymers were developed for ablation at a specific irradiation wavelength, i.e. 308 nm, to overcome these limitations [5–9]. Photochemical considerations have been applied for the design of these polymers. The irradiation wavelength of 308 nm was chosen because of the convenience of this wavelength from a practical point of view, i.e. lifetime of the optical components and gas fills of the XeCl excimer laser, and because sub-micron resolution is not necessary for all applications. For an irradiation wavelength of 308 nm, it is possible to selectively irradiate into the absorption band of the photochemically active chromophore, whereas other parts of the polymer, such as aromatic or aliphatic groups, absorb at shorter wavelengths. This can give indications about the role of the photochemically active chromophore during the ablation process and, therefore, the ablation mechanism. It is still not clear whether the ablation mechanism is purely photothermal or has at least partly photochemical features. The latter has been suggested for shorter irradiation wavelengths, e.g. 193 nm [10]. The most promising approach for the design of these 'laser ablation polymers' is the incorporation of the photochemically active chromophore into the polymer main chain. These polymers are highly absorbing

* Corresponding author. Tel.: +41-56-310-4076; fax: +41-56-310-2485.
E-mail address: thomas.lippert@psi.ch (T. Lippert).

1010-6030/01/$ – see front matter © 2001 Elsevier Science B.V. All rights reserved.
PII: S1010-6030(01)00577-9

at the irradiation wavelength and decompose exothermally at well-defined positions of the polymer chain into gaseous products [11]. The gaseous products act as driving gas of ablation and carry away larger fragments, which could otherwise contaminate the surface. The polymers are ablated without major modifications of the residual polymer surface [12], thus allowing reproducible ablation. These polymers contain photolabile groups (–N=N–X–) in the polymer backbone, which decompose upon laser irradiation. Various functional groups, such as X = –N<, –S–, –N–N=N–, or phosphonate, have been tested [7,8]. The triazene polymers (TC-polymers) with –N=N–N< as structural unit revealed most of the desired properties, e.g. formation of high quality films, stability to storage, and one-step synthesis [13]. The only major disadvantage of the TC-polymers is the sensitivity to acids [14], which are used in industrial applications for the following processing steps. Therefore, another class of polymers has been developed which are based on polyesters. The polymers contain cinnamylidenemalonic acid groups (CM-polymers) which undergo photocrosslinking upon irradiation at $\lambda > 395$ nm and laser ablation at 308 nm [15]. These polymers are stable in acids and can function as positive (laser ablation) as well as conventional negative resists. An application is envisioned where first a 'large' scale structuring, using standard negative resist methods, is followed by a positive (i.e. laser ablation) step to structure the remaining areas in more detail. The order of processing can be reversed without altering the quality of the structures [15]. Additionally, combined polymers were developed (TCCM-polymers) which contain the structure of the TC-polymers and CM-polymers. One polymer of each group (TC, CM and TCCM) was selected which revealed a high linear absorption coefficient of around 100 000 cm^{-1} at the irradiation wavelength. To compare the ablation properties of these photopolymers, a reference polymer was included in this study, i.e. polyimide, as representative of a highly absorbing 'standard' polymer (see Scheme 1).

We compared the ablation properties of these various polymers to investigate the ablation mechanism. One polymer (TC) was studied in more detail with additional analytical techniques (time-of-flight mass spectrometry) and other irradiation sources (excimer lamps). Additionally, novel applications of these photopolymers designed for laser ablations will be presented.

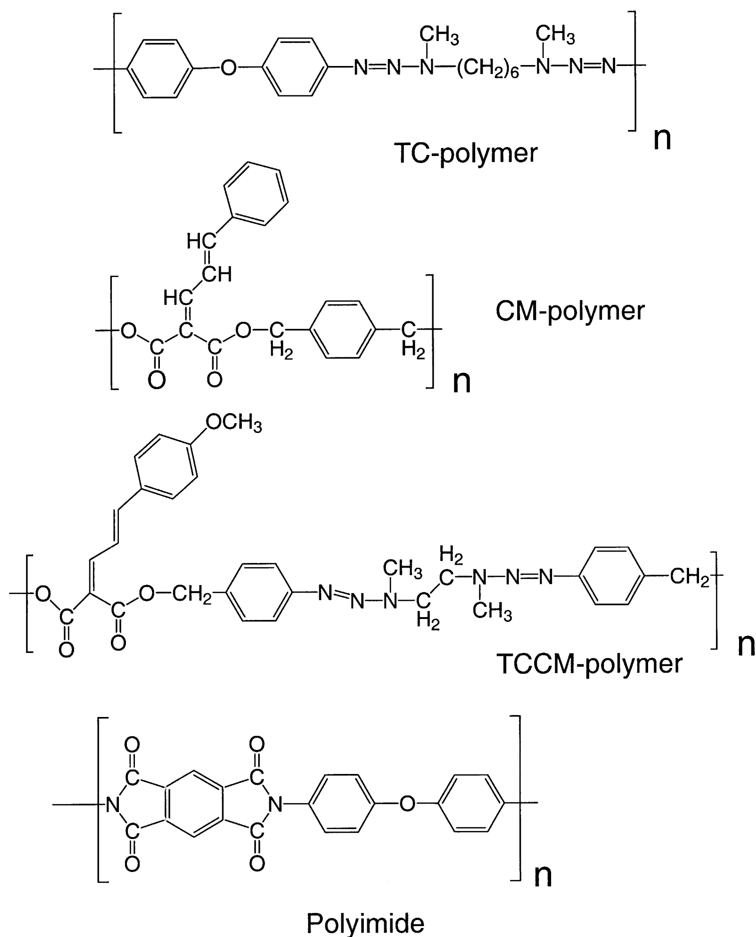

Scheme 1. Chemical structures of the polymers.

2. Experimental

The polymers, TC, CM and TCCM were synthesized using standard polycondensation reactions. The syntheses are described in detail elsewhere [16,17]. A XeCl excimer laser (Lambda Physik, Compex 205; $\lambda = 308\,\text{nm}$, $\tau = 20\,\text{ns}$) was used as irradiation source. The polymer films (50 μm thick) for the laser ablation experiments were prepared by solvent casting with THF or chlorobenzene as solvent. The samples for the excimer-lamp irradiation were prepared by spin coating. The procedure for determining the etch rates has been described in detail elsewhere [18]. The ablation experiments were performed at low (10–400 mJ cm^{-2}) fluences to investigate the ablation behavior of the polymers at fluence range where structural properties might be important.

The experimental arrangement for the time-of-flight mass spectrometer (TOF-MS) has been described previously [19]. The polymer films were irradiated at 248 and 308 nm at a pulse repetition rate of 1 Hz to avoid accumulative heating. Emitted fragments were detected with a quadrupole mass spectrometer (UTI 100C) mounted with the ionizer 14 cm from the sample. Time resolved quadrupole mass spectroscopy was used to simultaneously measure both the mass (amu) and the time-of-flight distributions of the emitted species.

Excimer lamps were used as an alternative source of excitation. The incoherent excimer radiation from a dielectric barrier discharge (silent discharge), operating in pure xenon, gas mixtures of krypton/chlorine and xenon/chlorine, provides intense narrow band radiation at $\lambda = 172\,\text{nm}$ (Xe_2^*), 222 nm (KrCl*) and 308 nm (XeCl*), respectively. The discharge was initiated in an annular gap between coaxial quartz tubes. The outer quartz tube had a diameter of 3 cm and an active length of 10 cm defined by the length of the grounded wire mesh acting as transparent outer electrode. The radial width of the annular gap was about 0.8 cm. The excimer UV sources were operated at frequencies between 125 and 375 kHz and voltage amplitudes up to 10 kV. More details about the excimer UV sources can be found in the literature [20,21]. The UV spectra after irradiation in Ar, air and oxygen were measured with a Varian Cary 500 spectrometer.

The microoptical elements were fabricated with gray tone phase masks, as described elsewhere [22,23]. The polyimide sheets (125 μm Kapton® from Goodfellow) and spincoated polyimide films (Durimide 7020, Arch Chemical) were used as received.

The tests with near-IR radiation for laser plasma thruster (LPT) application were performed with diode lasers. Experimental details and further information about this application can be found elsewhere [24,25].

3. Results and discussion

3.1. Ablation properties

Polymers with very similar linear absorption coefficient, α_{lin} (around 100 000 cm^{-1}, see Table 1) were selected to compare the ablation parameters. The etch rates (etch depth/pulse) at low fluences were calculated from linear plots of the etch depths vs. pulse number at a given fluence. All plots were linear, showing no incubation behavior as expected for highly absorbing polymers [26]. The high fluence range is mainly interesting for applications where high ablation rates in small areas are important, e.g. drilling or cutting. The ablation rates at high fluences are very similar for all polymers [27] and are of only minor importance for structure property relations. The low fluence range offers the opportunity to study the influence of structural parameters on the ablation rates. The dependence of the etch rates on the natural logarithm of the fluence are shown for all polymers in Fig. 1. The ablation parameters, α_{eff} (effective absorption coefficient) and F_{th} (threshold fluence) were calculated according to the following equation [28,29]:

$$d(F) = \frac{1}{\alpha_{\text{eff}}} \ln\left(\frac{F}{F_{\text{th}}}\right) \quad (1)$$

where $d(F)$ is the etch rate (etch depth per pulse). The calculated values for α_{eff} and F_{th} are summarized in Table 1. The effective absorption coefficient, which is a measure for the penetration depth of the laser photons is dependent on the applied laser fluence. The designed polymers (TC, CM and TCCM) can be divided into two groups with respect to the etch rates (shown in Fig. 1). All triazene containing polymers have significantly higher etch rates than the other polymers. The designed polyester (CM) reveals a higher etch rate than PI. The etch rates are independent of α_{lin} (see Table 1) and determined by the chemical structure. In Fig. 2, a comparison of the calculated etch rates at 100 mJ cm^{-2} and of the decomposition temperatures is shown for all polymers. The etch rates of the non-triazene containing polymer, CM, is 90 nm/pulse, which is about $\frac{1}{3}$ of the value of the triazene

Table 1
Chemical properties and ablation parameters of the polymers

	TC-polymer	CM-polymer	TCCM-polymer	Polyimide
α_{lin} (cm^{-1})	100000	102000	92000	95000
α_{eff} (cm^{-1})	50000	51000	53000	83000
F_{th} (mJ cm^{-2})	27	63	28	60
d (nm/pulse) at $F = 100\,\text{mJ cm}^{-2}$	267	90	239	61
Decomposition temperature (°C)	227	321	248	>500

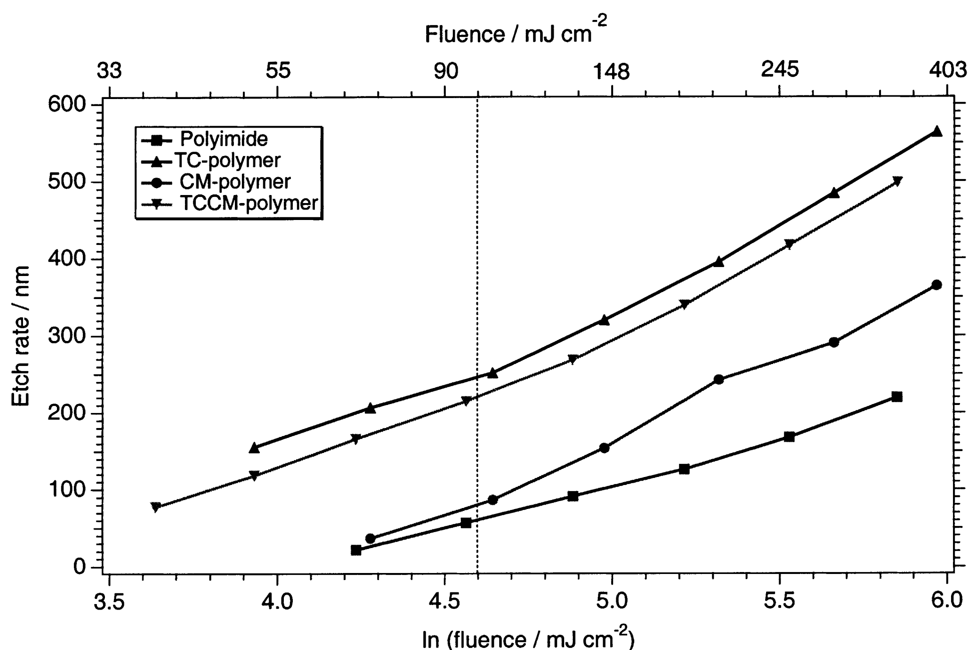

Fig. 1. Measured etch rates as a function of the natural logarithm of fluence at low fluences (up to 400 mJ cm^{-2}).

containing polymers, TC and TCCM. A slightly higher etch rate is obtained for TC, which has the highest triazene density per repetition unit. The etch rate of polyimide is about 60 nm/pulse which is again about $\frac{2}{3}$ of the value of the CM-polymer. Another important feature is the similarity of α_{eff} for all designed polymers (around 50 000 cm^{-1}), while polyimide reveals a much higher value (close to the linear absorption coefficient). The fact that all designed polymers have a similar effective absorption coefficient, but very different etch rates and threshold fluences, suggests that α_{eff} is only of minor importance for the ablation performance. The very similar effective absorption coefficient might be due to similar ablation products/intermediates in the polymer films. All designed polymers are supposed to decompose

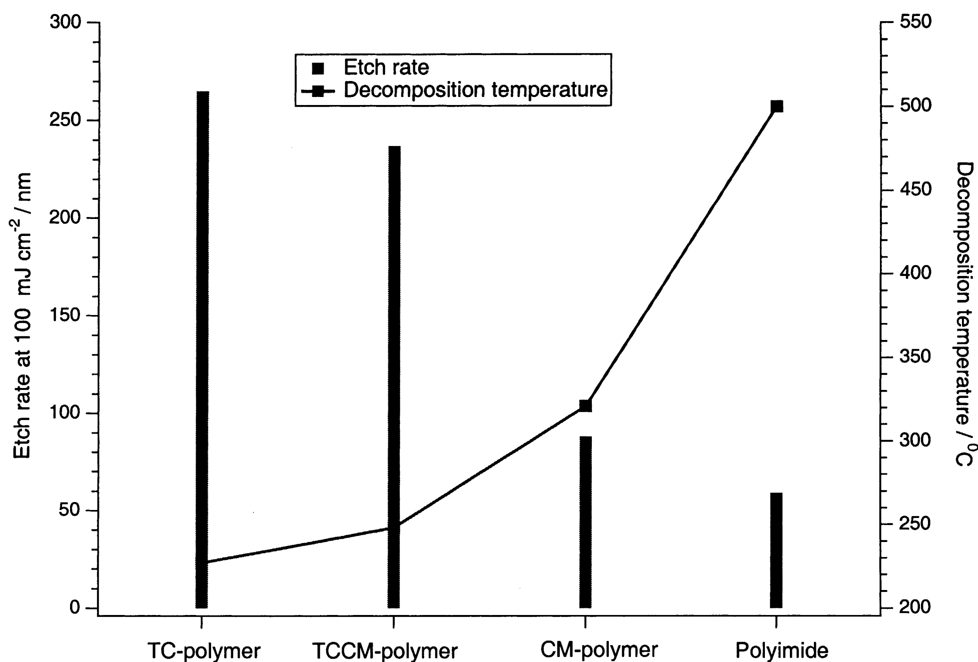

Fig. 2. Etch rates at 100 mJ cm^{-2} and decomposition temperatures of the polymers.

according to similar mechanisms (at least the initial steps), i.e. direct photolysis, during which homolytic bond breaking occurs [30,31]. Radicals are formed as intermediates, especially aromatic radicals, which should be present for all designed polymers. These common products/intermediates could be the reason for the very similar α_{eff}. In the case of polyimide, different intermediates with different absorptivities are formed, i.e. quite stable amide and isocyanate intermediates were detected by FT-IR spectroscopy [32].

The designed polymers reveal clearly better ablation properties that a standard, commercial polymer. All selected polymers had similar absorption properties and also common structural elements (aromatic groups) ensuring that a direct comparison of the polymers is possible. The polymers containing the group (triazene) with the highest photochemical activity (TC and TCCM) are also the materials with the best ablation performance. This suggests that photochemical properties of specific structural units determine the ablation behavior of polymers containing these groups.

Of course one might argue that the same order of activity is also obtained if only the decomposition temperatures (T_{dec}) are considered, i.e. lowest T_{dec} for the TC- and TCCM-polymer, followed by CM and then PI (Fig. 2). However, a comparison reveals that the largest difference in thermal stability (170°C) between polymers of different groups, i.e. PI and CM, corresponds to the smallest difference in ablation activity, while a much smaller difference in thermal stability (70°C), between TCCM and CM, corresponds to the largest difference in ablation activity. This is even more remarkable when recalling that this is valid in a broad fluence range (from 10 to at least 400 mJ cm^{-2}), which covers a quite broad thermal range. This suggests that thermal considerations are less important for the laser ablation of these polymers. Just using the decomposition temperatures is of course a simplification, because other parameters such as thermal conductivity, specific heat, thermal diffusivity, etc. are also important. Looking at the chemical structure of the polymers shows that, all polymers have at least common parts in their chemical structure suggesting that they might have comparable values for these constants, and hence justifying the simplification. Photolysis experiments in solution had given the same order of photochemical activity as in the ablation experiments [18], indicating that the photochemical activity is also important for the ablation behavior. This implies also that the ablation mechanism has pronounced photochemical aspects, at least for polymers containing photochemically active groups.

3.2. *Time-of-flight mass spectrometry*

For a better understanding of the ablation mechanisms of the designed photopolymers, one polymer was selected (TC) and studied in more detail with additional techniques. The TC-polymer was chosen, because it is the most active and most data are available for this polymer. An additional feature of this polymer is visible in the UV–Vis spectrum (Fig. 3). The absorption maximum is close to the irradiation wavelength of 308 nm, while an absorption minimum is at another excimer laser emission wavelength, i.e. 248 nm. A comparison of these two irradiation wavelengths, one corresponding to the absorption of the photochemical active triazene-group at 308 nm, the other to the photochemically more stable aromatic system, could give valuable information about the influence of these structural units on the ablation mechanism. As analytical method TOF-MS was selected, because different products of ablation, or intensities of products, can give a direct indication for a different ablation mechanism. Previous studies [33,34] with 248 nm and detailed analysis of the time-of-flight curves had shown that fragment emission follows an Arrhenius relation, where the temperature is predicted from the total deposited laser energy. For a direct comparison between the two irradiation wavelengths, the relative maximum peak intensities of different fragments are compared. In Fig. 4, the response of the

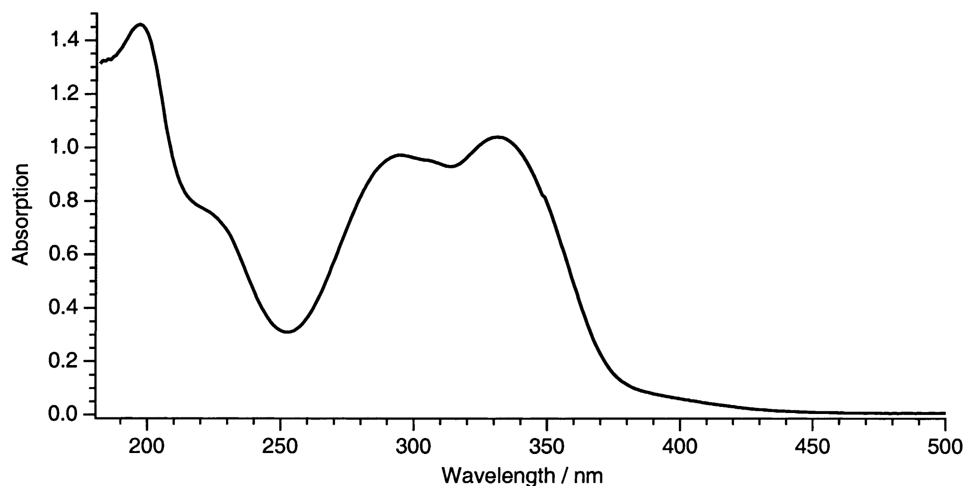

Fig. 3. UV–Vis absorption spectra of the TC polymers. This film coated from chlorobenzene onto a quartz wafer.

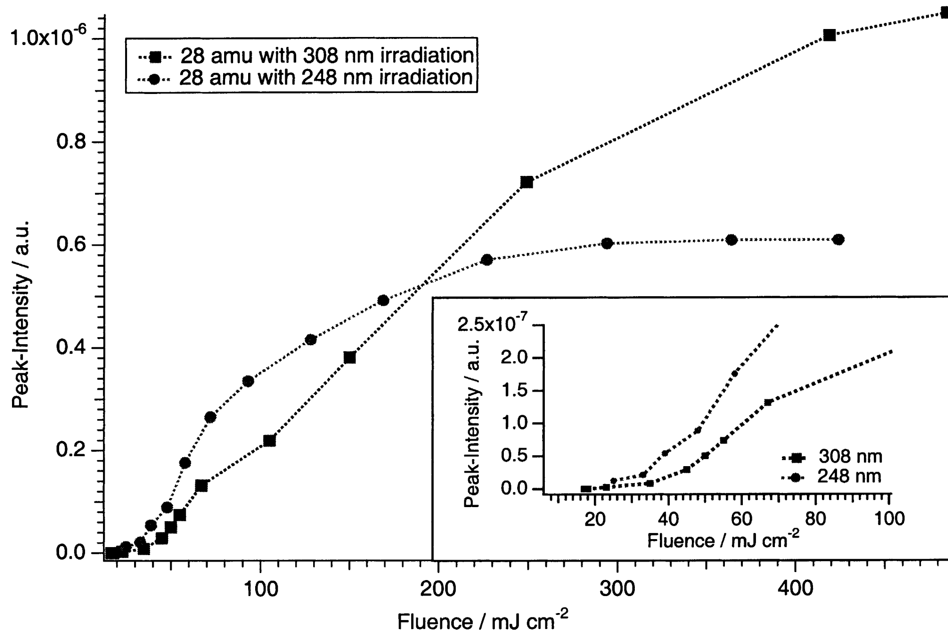

Fig. 4. Intensity of the 28 amu signal from decomposition of TC at various fluences with 248 and 308 nm irradiation.

most intense mass (i.e. 28 amu from N_2) at the two different irradiation wavelengths is compared. The data taken after irradiation at 308 nm exhibit a linear increase of the signal intensities at low fluences ($<$40 mJ cm^{-2}), as shown in the inset in Fig. 4. At higher fluences, a fast increase is observed. This is an indication that at fluences above $\sim$40 mJ cm^{-2}, the process changes from a linear photochemical reaction to the non-linear ablation process. This value agrees very well with the ablation threshold of $\sim$25–30 mJ cm^{-2}, which was determined with other techniques [35,36].

After irradiation at 248 nm, a much faster increase of the signal was detected and no linear range can be observed (see inset in Fig. 4). At higher fluences, the signal intensity reaches a maximum. This is probably due to absorption of the incoming photons by aromatic fragments (e.g. radicals, which are produced during ablation). In Fig. 5, the observations for other analyzed masses after irradiation at 308 nm are summarized. Only signals were analyzed which can be assigned to direct laser ablation products (see Scheme 2), maybe with the exception of mass 76/77, which could be

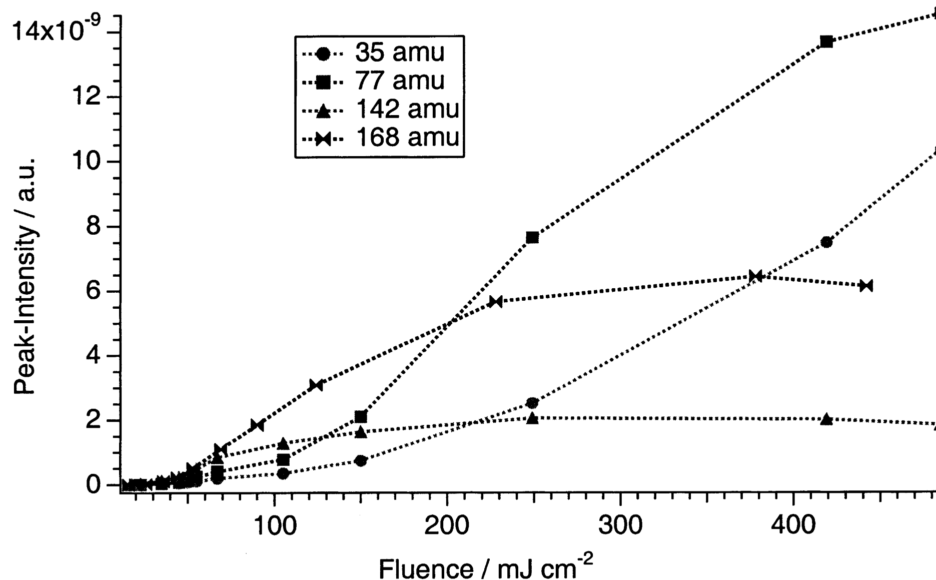

Fig. 5. Intensity of the other fragments from decomposition of TC at various fluences with 308 nm irradiation.

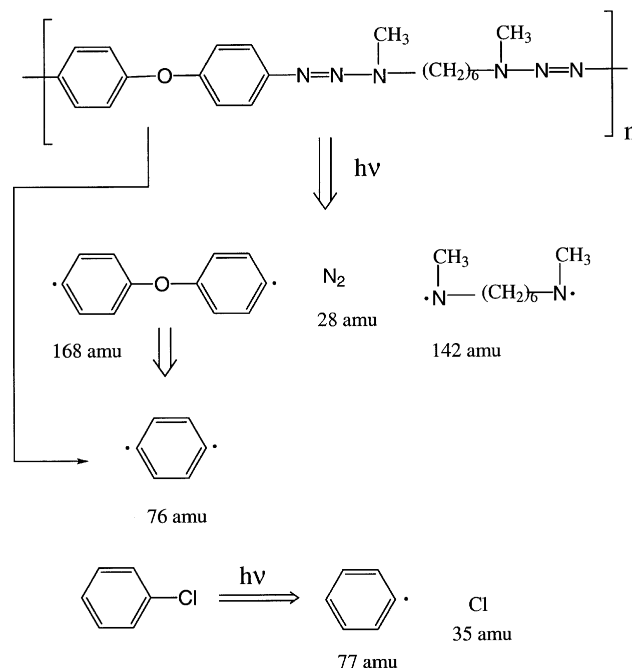

Scheme 2. Fragmentation pattern of the TC-polymer.

a primary product of laser ablation, but also a fragment of the electron impact or of reactions in the ablation plume. The resolution of our experimental set-up does not allow to distinguish between these two masses.

A tentative interpretation of the signal is as follows. The fragment with the mass 35 (fragment of the solvent chlorobenzene that cannot be removed totally from the films) is non-linearly increasing over the whole fluence range; chlorobenzene probably contributes also to the 76/77 amu signal. At low fluences, the signal is quite low and increases significantly at fluences above 150 mJ cm^{-2}. This can be explained with a surface region which contains less solvent than the deeper layers [37]. As the fluence increases, the depth of the ablated crater increases and more solvent is removed. The fragment with the mass 76/77 results from the fragmentation of the solvent and from the decomposition of the 168 amu fragment (cf. Scheme 2). At lower fluences, the 76/77 amu signal seems to be correlated with the 35 amu signal, while it starts to increase more rapidly in the fluence range where the 168 amu signal levels off. The 168 fragment decreases at higher fluences and an increase of the 76/77 amu signal is detected. The 142 amu fragment intensity increases initially, similar to the 28 amu signal, suggesting that both are products of the same process. At higher fluences, the signal intensity stays constant, probably due to the decomposition of this fragment. The 168 amu signal reveals a similar behavior as the 142 amu signal.

In Fig. 6, the signal intensities of the same masses are shown for 248 nm irradiation. The 35 amu signal intensity increases slowly at the beginning and much faster at the high fluence end. This can again be due to a dense surface region with a lower amount of solvent, which has been previously found for PMMA cast from chlorobenzene [37]. Other possibilities are the higher ablation rates at higher fluences, which result in higher Cl signals, or a more effective decomposition of the chlorobenzene at higher fluences. The 76/77 amu signal increases slowly at the beginning, but when the fluence reaches the value where the 168 signal decreases, a fast increase is observed. At still higher fluences, the phenyl fragment signal decreases again, most probably due to decomposition. This is only observed for 248 nm irradiation. The higher photon energy at 248 nm is sufficient to decompose the aromatic system, causing a decrease of the signals related to the aromatic fragment. The 142 amu signal increases at low fluences, until it reaches a certain maximum. Then it decreases slowly to reach a constant value. This behavior can again be explained by a decomposition of this fragment at higher fluences (similar to 308 nm irradiation).

In comparison, pronounced differences between the signal intensities at 248 and 308 nm irradiation are observed. The fragments with masses higher than 35 reveal clearly higher intensities for 308 nm irradiation. This is due to the higher etch rates at 308 nm [5] at higher fluences, but also to further decomposition of the larger fragments with the higher photon energy of the 248 nm irradiation. At lower fluences, especially in the case of N_2, higher intensities are detected for 248 nm. For 308 nm irradiation, a linear behavior of the signal with the laser fluence can be observed. Around the threshold of ablation, this linear behavior changes, i.e. faster increase of the signal intensity. As argued above, we observe the photochemical decomposition of the triazene-polymer with 308 nm irradiation at low

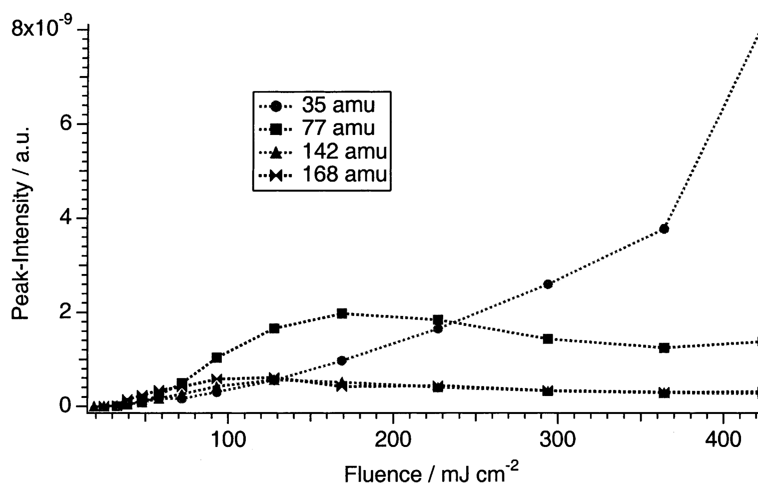

Fig. 6. Intensity of the other fragments from decomposition of TC at various fluences with 248 nm irradiation.

fluences. The triazene group ($N^1{=}N^2{-}N^3{<}$) decomposes photochemically between the N^2 and N^3 nitrogen atoms, and N_2 is released (shown in Scheme 2). The other radical fragments of this homolytic decomposition of the N–N bond are combining to form an insoluble crosslinked polymer network, as described in the next paragraph in more detail. The available experimental data do not really show this linear relation for 248 nm irradiation at low fluences, may be due to the low intensities of the N_2 fragment.

3.3. Excimer-lamp irradiation

Excimer lamps were applied to study the low fluence irradiation region, where linear (no ablation) photochemistry is taking place. This is in the fluence range (e.g. Fig. 4 inset), where a linear relation between reaction products and laser fluence is observed. The excimer lamps emit at the same wavelength as the excimer laser, but with incoherent radiation, and in quasi-CW mode. The peak photon fluxes of the lamps are also low compared to the excimer laser, suggesting that multi-photon processes are not important. Thin films of the TC-polymer on quartz substrates were irradiated with the excimer lamps under different conditions, i.e. in Ar, air and O_2. As irradiation source, XeCl (308 nm), KrCl (222 nm) and Xe_2 (172 nm) excimer lamps were selected. Excimer lamps based on fluorine containing excimers are difficult to operate, due to etching of the quartz housing by the F_2. Therefore, the KrCl excimer lamp was used instead of the KrF 248 nm irradiation, and additionally the Xe_2 excimer lamp. Different atmospheres were used for the 172 nm irradiation, because oxygen has a strong absorption band around 172 nm and ozone, oxygen radicals and excited molecular oxygen species are formed upon irradiation [38]. These reactive oxygen species cause photooxidation, in addition to the direct photolytic decomposition of the polymer. The irradiations at 308 and 222 nm were carried out in air. Effective direct etching of polymers by excimer lamps can only be observed at reduced pressures (between 0.1 and 100 mbar) [39] which was not examined in this study, where only atmospheric pressure was applied. The thin polymer films were irradiated for certain time periods, followed by analysis with the UV–Vis spectrometer. The decomposition of the polymer was analyzed at the two maxima, i.e. 196 and 330 nm. The former corresponds mainly to the absorption of the aromatic groups, the latter to the triazene groups [35].

With 308 nm irradiation nearly exclusively decomposition of the triazene-group (330 nm) can be observed. Only very minor changes are observed for the band at 196 nm. This is shown in Figs. 7 and 8 where the changes of the two absorption maxima are plotted as a function of the irradiation time for all irradiation wavelengths. A detailed analysis of the changes of the band at 196 nm (Fig. 8) reveals an instant drop of intensity for all irradiation wavelengths. The reasons for this behavior are not clear, but it might be due to desorption of adsorbed species or most probably to the temperature increase of the polymer surface upon irradiation with the hot lamp. After this initial decrease of intensity, an increase can be observed. This increase is clearly visible for all irradiation wavelengths, but is most pronounced for irradiation at 222 nm. It might be caused by an increase of the molecular weight of the polymer (crosslinking), which has also been detected after thermolysis of the polymer in substance [40]. The crosslinking can be explained by the photochemical decomposition mechanism of the polymer (Scheme 2). Radical species are created upon the homolytic bond scission of the N–N bond. In the next step, nitrogen is eliminated and the radicals combine to form a crosslinked polymer. This crosslinked polymer is insoluble and the whole process is comparable to the processing of a negative photoresist. The photon energy (4.02 eV) of the 308 nm excimer lamp has enough energy to break the N–N bond (1.7 eV), but the energy is only slightly above the binding energy of C–C bonds (3.6 eV) and clearly below the energy of a C=C bond (6.36 eV). The binding energies of the bonds in the aromatic

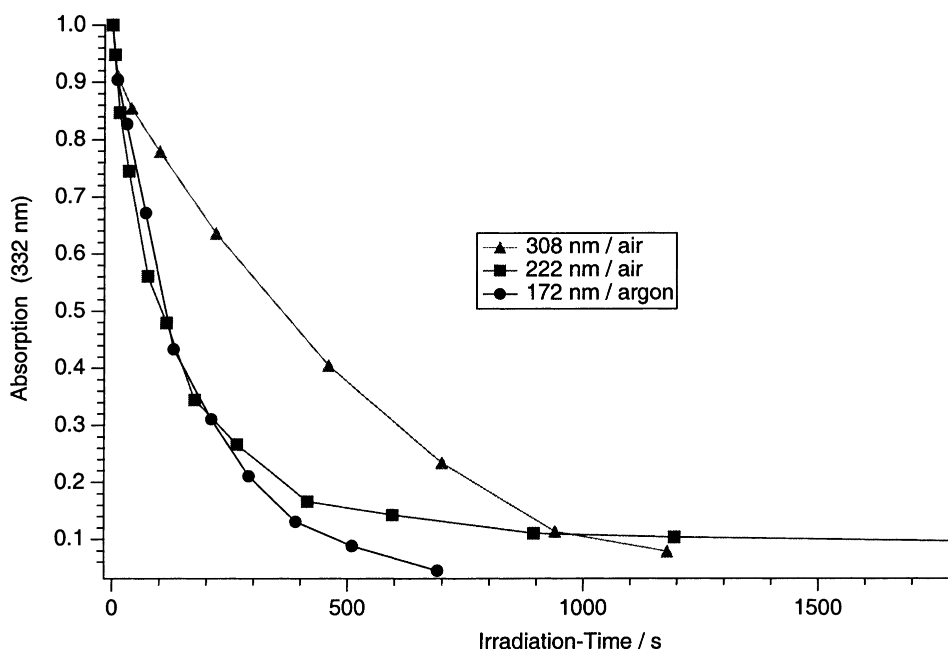

Fig. 7. Change of the absorption at 332 nm at various irradiation times with 172, 222 and 308 nm. The irradiation was performed in air for 308 and 222 nm wavelengths, and in Ar for 172 nm. The absorption was normalized to 1 for all experiments.

systems, which are probed at 196 nm, should be somewhere between these values. This explains why only small changes of the band at 196 nm are detected for 308 nm irradiation.

In the case of 222 nm irradiation, both bands are decreasing. As expected, a faster decrease of the 330 nm band is observed, compared to 308 nm irradiation (Fig. 7). The excitation of electronic transitions is not localized, and a fast redistribution of the energy takes place, resulting not only in the decomposition of groups that are directly related to the irradiation wavelength. In other words, it is expected that with irradiation at 222 nm (or 172 nm) the most labile bond, i.e. the triazene group is broken first. The higher photon energy of the 222 nm photons (5.58 eV) is more effective for the decomposition of the N–N bond, resulting in the faster

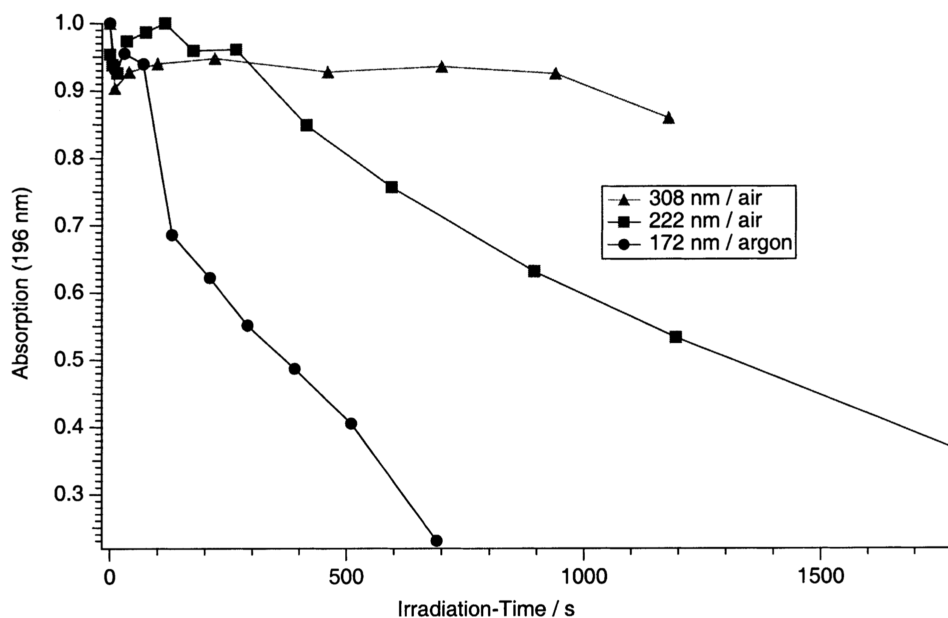

Fig. 8. Change of the absorption at 196 nm at various irradiation times with 172, 222 and 308 nm. The irradiation was performed in air for 308 and 222 nm irradiation and in Ar for 172 nm. The absorption was normalized to 1 for all experiments.

decomposition of the triazene group, i.e. band at 330 nm (Fig. 7). Contrary to 308 nm irradiation, the band at 196 nm is, also decreasing with 222 nm irradiation (Fig. 8). This can only be observed after an initial increase and a period of nearly constant absorption. The increase of absorption and the constant range can be explained by the above-described crosslinking of the polymer. These crosslinked structures could have a higher absorption coefficient at 196 nm than the starting material. The energy of the 222 nm photons is high enough to decompose the aromatic system, and, therefore, to destroy the newly created crosslinked structures. As long as many new radicals are formed upon the decomposition of the triazene group and crosslinking takes place, a quasi-steady-state between decomposition and creation of crosslinked structures exists. This is the range of nearly constant absorption of the band at 196 nm. After about 250 s of irradiation, when around 80% of the triazene groups are decomposed, more crosslinked groups are decomposed than formed and the absorption decreases.

The irradiation at 172 nm results in the fastest decomposition of both bands. In Figs. 7 and 8, the changes upon irradiation in Ar is shown, because under these conditions, additional effects of oxygen, as described below, are omitted. Again, an initial increase of the band at 196 nm (Fig. 8) is observed, but is followed by a quite fast decrease. This can be explained by the high photon energy (7.2 eV) of the 172 nm radiation, which can directly break all bonds in a polymer. The decomposition of the polymer upon 172 nm irradiation is dependent in addition on the atmosphere in the irradiation chamber. The fastest decomposition is observed in air, followed by oxygen and argon. The 172 nm radiation is absorbed by the oxygen in the reaction chamber, and ozone, oxygen radicals and excited molecular oxygen species are formed [39]. These species are very reactive and decompose the polymer. This process was described previously as photooxidative decomposition [41], which can also result in etching at atmospheric pressure. We observed etch rates of ~5.5 nm min^{-1} in air which is comparable to etch rates reported for other polymers (1–5 nm min^{-1}) [39,41]. This additional decomposition path is absent in Ar, resulting in the slowest decomposition rates. In pure oxygen, on the other hand, the radiation is absorbed close to the lamp, where the reactive species are formed. Therefore, less reactive species and photons are reaching the polymer surface in O_2. As a result, the fastest decomposition of the polymer is observed in air.

The excimer-lamp irradiation experiments show clearly that photochemical decomposition of the TC-polymer takes place, even at low fluences and quasi-CW irradiation (the excimer lamps emit burst of UV pulses with ns duration, but with repetition frequencies in the kHz range). The results are summarized in Fig. 9, where the inverse half-life periods of the two bands at the different irradiation wavelengths are shown. It is clearly visible that with 308 nm irradiation, only the triazene band at 330 nm decreases, while for all other irradiation wavelengths, both bands are decreasing. The irradiation wavelength with the highest photon energy results in the fastest decomposition of both bands. For irradiation at 172 nm, a pronounced influence of the atmosphere can be observed. Irradiation in air results in the fastest decomposition of the band at 196 and 330 nm, due to oxidative decomposition of the polymer by the above-described reactive oxygen species. Upon irradiation with 308 nm and in the early stages of the irradiation at 222 nm, an insoluble polymer network is formed. A quantitative comparison of the half-life periods between the different irradiation wavelength

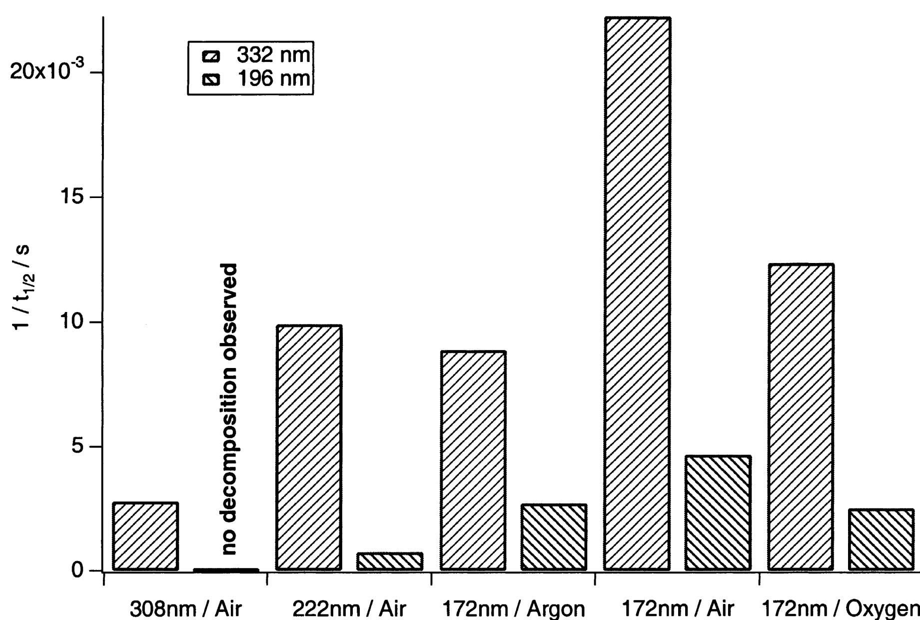

Fig. 9. The inverse half-life times of the 196 and 332 nm absorptions with all irradiation wavelengths and under all conditions.

is not possible, due to the different irradiation doses. It is also noteworthy to mention that the irradiation is accompanied by a temperature increase (<100°C), due to the temperature of the excimer lamps.

3.4. Novel applications

3.4.1. Microoptical elements

Laser ablation can be used to create complex patterns, e.g. microoptical elements. This can be accomplished by scanning ablation tools [42], which are even capable of producing continuous topographies by varying the applied fluence on the material surface. Due to the sequential nature of the method, the throughput is very limited. A parallel patterning of larger areas requires a set-up comparable to photo steppers, where the mask structure is projected onto the substrate surface [43]. One of the major problems of this method is the damage occurring in chromium absorber structures of standard photomasks at higher laser fluences [44]. An alternative technique utilizes diffractive grating structures etched into a quartz mask blank to diffract the transmitted light out of the aperture of the projection optics [23,45]. This method combines the capability of scanning ablation tools to vary the ablated depth continuously with high throughput of projection methods. An additional improvement can be achieved by the application of our special photopolymers, e.g. TC-polymer. An example of microstructures, i.e. Siemens stars, etched into the TC-polymer and polyimide are shown in Fig. 10. The Siemens star is used to check the ablation resolution and to find the focal point for ablation. The modified and re-deposited material is clearly visible around the ablated structure of the polyimide (Fig. 10, top left), but is absent for the triazene-polymer. Any surface contamination or modification will deteriorate the performance of the microoptical elements and render the ablation rates unpredictable. In the case of polyimide, redeposited material is also clearly visible inside the ablated structure (Fig. 10, bottom left), while the structure in the TC-polymer is better defined with no debris. The higher sensitivity and etch rates of the triazene-polymer allows the application of larger phase masks, or less pulses are necessary to fabricate an optical element with a given depths of the structures. The structures in Fig. 10 are obtained with 2 pulses for the triazene-polymer, while for the polyimide more than 5 pulses were necessary to achieve similar ablation depths.

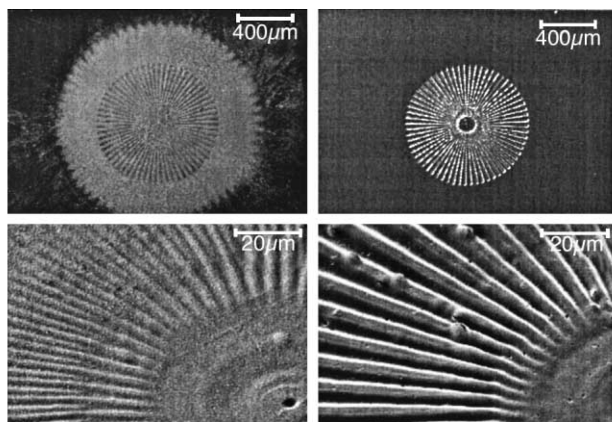

Fig. 10. SEM images of Siemens stars fabricated by laser ablation. Top: Siemens stars in polyimide (left) and in the triazene-polymer (right) using 5 pulses. Bottom: magnification of the Siemens stars in the top row.

The combination of gray tone phase masks with the highly sensitive photopolymers is suitable for the fast fabrication of three-dimensional topographies. Single laser pulses can create complex structures, such as Fresnel lenses. A pattern transfer into glass or quartz, e.g. by proportional etching techniques, would open an even larger spectrum of applications.

3.4.2. Near-IR irradiation for LPT

A very different application of laser ablation of polymers can be found in aerospace science. With the advent of microsatellites (>10 kg), nanosatellites (1–10 kg) and even picosatellites (<1 kg), it is necessary to develop steering engines which have a small mass (~200 g) and size, produce a high specific impulse, and are inexpensive [25]. One promising candidate for this application are LPTs, which have some advantages over more common candidates for microthrusters, such as pulsed plasma thrusters or resistojets [25]. Due to the specific demands, i.e. weight and power, of small satellites, small powerful (~1 W) diode laser must be used. These lasers emit in the near-IR (930–980 nm), with an available power of around 1–5 W and pulse lengths from 100 μs to the ms range. Fluences of several 100 J cm^{-2} can be achieved with standard optical components (laser spot diameter around 5 μm). The long pulse lengths of the diode lasers restrict the applicable materials to polymers, which have low thermal conductivities. The performance of the LPTs is to a large extent depending on the properties of the polymers used in these devices. The well-defined exothermic decomposition of the TC-polymer was an attractive feature to test these polymers also for an application with near-IR irradiation.

To analyze the performance of polymer films for LPTs, the target momentum was measured by a special developed torsion balance [25]. The target momentum is used to calculate the momentum coupling coefficient, C_m. This quantity is defined as

$$C_m = \frac{m\Delta v}{W}$$

with $m\Delta v$ as target momentum produced during the ejection of laser-ablated material. W is the incident laser pulse energy.

Most polymers have to be doped to accomplish an effective absorption in the near-IR. Carbon was chosen as dopant due to the broad homogenous absorption over the whole near-IR range. Thin films of two doped polymers, i.e. TC-polymer and poly-vinylalcohol as an example for a

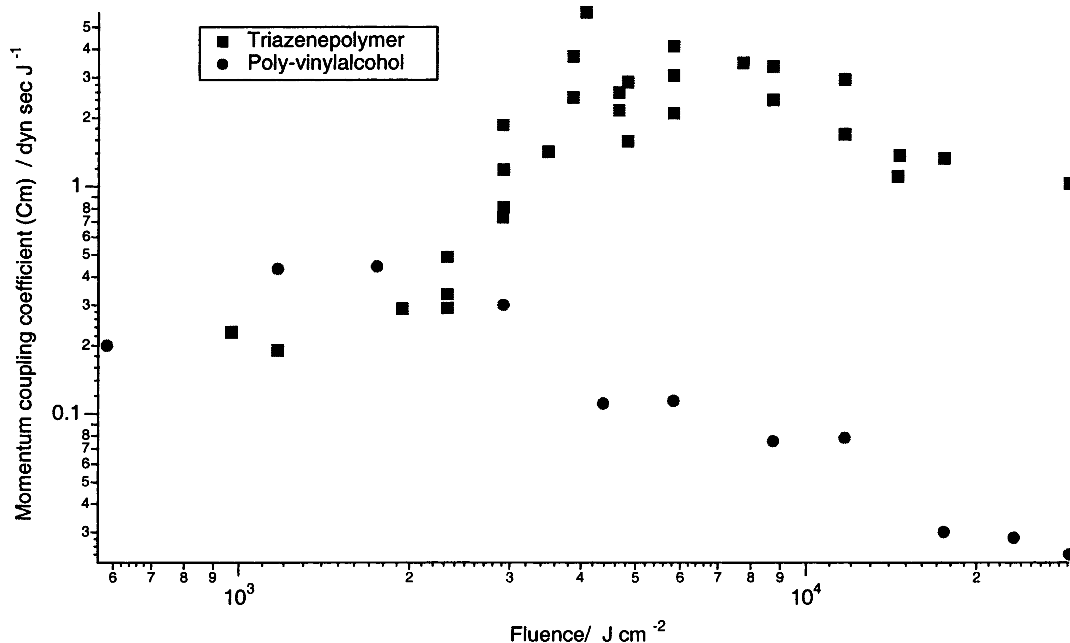

Fig. 11. Momentum coupling coefficients (impulse/laser energy) at various fluences for the carbon-doped polymers. Optical density of ~0.9 at 935 nm, film thickness ~65 μm, PET substrates.

commercial polymer, were prepared with an optical density of ~0.9 and a thickness of around 60 μm.

In Fig. 11, the momentum coupling coefficients at various laser fluences of the two polymers are shown. The triazene-polymer reveals higher coupling coefficients and more important, a quite well-defined threshold for a maximum C_m. The well-defined threshold and higher C_m of the triazene-polymer is an important feature for the design of a plasma thruster with tape-like polymer fuel, because the optimum incident laser fluence and tape speed are clearly defined.

4. Conclusions

The ablation characteristics of various polymers were studied at low fluences. The polymers can be divided into three groups, polymers containing triazene groups, polyesters with cinnamylidenemalonyl groups, and polyimide as reference polymer. The polymers containing the photochemically most active group (triazene) are also the polymers with the lowest threshold of ablation and the highest etch rates, followed by the designed polyesters and then polyimide. No pronounced influences of the absorption coefficients, neither α_{lin} nor α_{eff}, on the ablation characteristics are detected. The thermal properties of the designed polymers are only of minor importance. The clear difference between PI and the designed polymers might be explained by a pronounced thermal part in the ablation mechanism of PI, while photochemical activities are more important for the triazene-polymer. The time-of-flight mass spectrometry measurements show differences between irradiation at the absorption wavelength of the triazene group (308 nm) and irradiation at a shorter wavelength (248 nm). A linear range for the detection of the main ablation product, N_2, can be observed for 308 nm irradiation and the change from linear to non-linear behavior coincides with the ablation threshold. Larger fragments show lower intensities for 248 nm irradiation, due to the additional decomposition of these fragments, which most probably are absorbing at 248 nm and not at 308 nm, by the higher photon energy and the lower etch rates for 248 nm irradiation. The triazene group decomposes photochemically with excimer-lamp irradiation at 308 nm, without major decomposition of the aromatic groups. The resulting crosslinked polymer is insoluble in most common solvents. Irradiation with shorter wavelengths (222 and 172 nm) results in subsequent decomposition of the aromatic system. With 172 nm irradiation, the fastest decomposition of the polymer is detected. The decomposition is most effective in air where reactive oxygen species, such as radicals, cause additional photooxidative decomposition.

The combination of phase masks and specially designed, highly sensitive photopolymers can be used for an efficient fabrication of three-dimensional topographies using laser ablation. The application of the triazene-polymer, which has a very low threshold fluence, a high ablation rate and decomposes without contamination of the surface, allows a fast fabrication of microoptical elements. The triazene-polymer also reveals superior properties for applications in the near-IR. The carbon-doped polymer shows higher values of the momentum coupling coefficient (impulse of ablated products divided by laser energy) compared to a commercial polymer

(PVAlc). The well-defined threshold for the momentum coupling coefficient is an important feature for the application of polymers in LPTs for microsatellites.

Acknowledgements

This work has been supported be the Swiss National Science Foundation, a NATO Grant for international collaboration (CRG 973063), and by the US Air Force Office of Scientific Research (STTR Phase II Contract No. F49620-98-C-0038). BASF and BAYER have made some materials available. The authors would like to thank M. Gross, PSI, for the SEM investigation.

References

[1] R. Srinivasan, V. Mayne-Banton, Appl. Phys. Lett. 41 (1982) 576.
[2] Y. Kawamura, K. Toyoda, S. Namba, Appl. Phys. Lett. 40 (1982) 374.
[3] K. Suzuki, M. Matsuda, T. Ogino, N. Hayashi, T. Terabayashi, K. Amemiya, Proc. SPIE 2992 (1997) 98.
[4] F. Raimondi, S. Abolhassani, R. Brütsch, F. Geiger, T. Lippert, J. Wambach, J. Wei, A. Wokaun, J. Appl. Phys. 88 (2000) 1.
[5] T. Lippert, J. Stebani, J. Ihlemann, O. Nuyken, A. Wokaun, Angew. Makromol. Chem. 206 (1993) 97.
[6] T. Lippert, J. Stebani, J. Ihlemann, O. Nuyken, A. Wokaun, J. Phys. Chem. 97 (1993) 12296.
[7] T. Lippert, T. Kunz, C. Hahn, A. Wokaun, Recent Res. Dev. Macromol. Res. 2 (1997) 121.
[8] O. Nuyken, U. Dahn, N. Hoogen, D. Marquis, M.N. Nobis, C. Scherer, J. Stebani, A. Wokaun, C. Hahn, Th. Kunz, T. Lippert, Polym. News 24 (1999) 257.
[9] O. Nuyken, C. Scherer, A. Baindl, A.R. Brenner, U. Dahn, R. Gärtner, S. Kaiser-Röhrich, R. Kollefrath, P. Matusche, B. Voit, Prog. Polym. Sci. 22 (1997) 93.
[10] S. Küper, J. Brannon, K. Brannon, Appl. Phys. A 56 (1993) 43.
[11] L.S. Bennett, T. Lippert, H. Furutani, H. Fukumura, H. Masuhara, Appl. Phys. A 63 (1996) 327.
[12] T. Lippert, T. Nakamura, H. Niino, A. Yabe, Macromolecules 29 (1996) 6301.
[13] J. Stebani, O. Nuyken, T. Lippert, A. Wokaun, Macromol. Chem., Rapid Commun. 14 (1993) 365.
[14] T. Lippert, J. Wei, A. Wokaun, N. Hoogen, O. Nuyken, Appl. Surf. Sci. 168 (2000) 270.
[15] T. Lippert, J. Wei, A. Wokaun, N. Hoogen, O. Nuyken, Macromol. Mater. Eng. 283 (2000) 140.
[16] O. Nuyken, J. Stebani, T. Lippert, A. Wokaun, A. Stasko, Macromol. Chem. Phys. 196 (1995) 739.
[17] N. Hoogen, O. Nuyken, J. Polym. Sci. Polym. Chem. 38 (2000) 1903.
[18] T. Lippert, J. Wei, A. Wokaun, N. Hoogen, J. Phys. Chem. B 105 (2001) 1267.
[19] J.J. Shin, D.R. Ermer, S.C. Langford, J.T. Dickinson, Appl. Phys. A 64 (1997) 7.
[20] B. Eliasson, U. Kogelschatz, Appl. Phys. B 46 (1988) 299.
[21] U. Kogelschatz, Pure Appl. Chem. 62 (1990) 1667.
[22] C. David, D. Hambach, Microelect. Eng. 46 (1998) 219.
[23] C. David, J. Wei, T. Lippert, A. Wokaun, Microlectron. Eng. 57–58 (2001) 453.
[24] C.R. Phipps, J. Luke, Proc. SPIE 4065 (2000) 801.
[25] C. Phipps, J. Luke, Diode laser-driven microthrusters: a new departure for micropropulsion, AIAA Journal, 40 (1), January 2002.
[26] R. Srinivasan, B. Braren, K.G. Casey, J. Appl. Phys. 68 (1990) 1842.
[27] J. Wei, N. Hoogen, T. Lippert, Ch. Hahn, O. Nuyken, A. Wokaun, Appl. Phys. A 69 (1999) S849.
[28] J.E. Andrews, P.E. Dyer, D. Forster, P.H. Key, Appl. Phys. Lett. 43 (1983) 717.
[29] R. Srinivasan, B. Braren, J. Polym. Sci. 22 (1984) 2601.
[30] T. Lippert, J. Stebani, O. Nuyken, A. Stasko, A. Wokaun, J. Photochem. Photobiol. A 78 (1994) 139.
[31] A. Stasko, V. Adamcik, T. Lippert, A. Wokaun, J. Dauth, O. Nuyken, Makromol. Chem. 194 (1993) 3385.
[32] E.E. Ortelli, F. Geiger, T. Lippert, J. Wei, A. Wokaun, Macromolecules 33 (2000) 5090.
[33] T. Lippert, A. Wokaun, S.C. Langford, J.T. Dickinson, Appl. Phys. A 69 (1999) S655.
[34] T. Lippert, S.C. Langford, A. Wokaun, S. Georgiou, J.T. Dickinson, J. Appl. Phys. 86 (1999) 7116.
[35] T. Lippert, L.S. Bennett, T. Nakamura, H. Niino, A. Ouchi, A. Yabe, Appl. Phys. A 63 (1996) 257.
[36] T. Lippert, L.S. Bennett, T. Nakamura, H. Niino, A. Yabe, Appl. Surf. Sci. 96–98 (1996) 601.
[37] T. Lippert, R.L. Webb, S.C. Langford, J.T. Dickinson, J. Appl. Phys. 85 (1999) 1838.
[38] B. Eliasson, U. Kogelschatz, OZONE Sci. Eng. 13 (1991) 356.
[39] J.Y. Zhang, H. Esrom, U. Kogelschatz, G. Emig, Appl. Surf. Sci. 69 (1993) 299.
[40] O. Nuyken, J. Stebani, T. Lippert, A. Wokaun, A. Stasko, Macromol. Chem. Phys. 196 (1995) 751.
[41] R. Srinivasan, S. Lazare, Polymer 26 (1985) 1297.
[42] N.H. Rizvi, P.T. Rumsby, M.C. Gower, Proc. SPIE 3898 (1999) 240.
[43] E.C. Harvey, P.T. Rumsby, Proc. SPIE 46 (1998) 26.
[44] J.T. Yeh, Proc. SPIE 922 (1988) 461.
[45] R.S. Patel, W.H. Advocate, S. Mukkavilli, Int. J. Microcircuits Electr. Pack. 14 (1995) 388.